

Characterization of Ultrashort Laser Pulses Generated via Hollow-Core Fiber Compression

DESY Summer Student Program – Project Report

Philipp Rosenzweig
Friedrich-Alexander-Universität Erlangen-Nürnberg

September 8, 2015

Ultrafast Optics and X-Ray Division
Center for Free-Electron Laser Science – CFEL
DESY Hamburg



Supervised by Dr. Shaobo Fang and Dr. Liwei Song

Abstract

In this Summer Student Project, the generation of high-energy, ultrashort laser pulses based on a carrier-envelope phase-stabilized Ti:sapphire system has been examined. Using a self-constructed f - $2f$ interferometer, a carrier-envelope phase stability of 550 mrad root mean square has been demonstrated over 2 s. Slow carrier-envelope phase drifts could however be identified on a longer timescale, which can readily be attributed to the lack of a slow feedback loop acting on the laser amplifier. The 30 fs pulses delivered by the Ti:sapphire system were spectrally broadened inside a neon-filled hollow fiber. Dominated by self-phase modulation, the bandwidth increased by almost one order of magnitude to above 10^{15} rad/s. The generated bandwidth was found to exponentially depend on the gas pressure, indicating that the pulse propagation inside the fiber is considerably influenced by further processes beyond self-phase modulation and dispersion, which have yet to be identified. When the pulses copropagated with their frequency-doubled replicas, a further increase in bandwidth of 30 % has been observed, which can be attributed to cross-phase modulation between the pulses of different color. Employing frequency-resolved optical gating, the spectrally broadened and compressed pulses have been reconstructed with a full width at half maximum duration of 7.1 fs, close to the computed transform limit of 5.9 fs. This is, to the best of the author's knowledge, the shortest pulse duration generated with the present setup. The spectrotemporal pulse characterization is substantiated by a good agreement between the measured and retrieved spectrum, while the temporal and spectral phase turned out to be flat over the respective region of interest.

Table of Contents

Abstract	2
1 Introduction	3
2 Physical Principles and Techniques	4
2.1 Self- and Cross-Phase Modulation in Hollow-Core Fiber Compression .	4
2.2 Frequency-Resolved Optical Gating	6
2.3 Carrier-Envelope Phase and f - $2f$ Interferometry	7
3 Experimental Setup	9
4 Results and Discussion	10
4.1 Spectral Broadening inside the Hollow-Core Fiber	10
4.2 Spectrotemporal Pulse Characterization	12
4.3 Carrier-Envelope Phase Fluctuations	13
5 Summary and Outlook	15
References	16
Acknowledgements	17

1 Introduction

Stimulated by the invention of the laser in 1960 [1] and the subsequent discovery of mode locking [2], the field of ultrafast optics has ever since been subject to constant progress towards high-energy laser pulses of shorter and shorter durations, comprising only a few oscillation cycles of the carrier wave. As per the Fourier theorem, the latter have to be supported by a very broad spectrum, hence presenting a challenge to commercial table-top laser sources [3]. Being nonetheless vital for cutting-edge research in attoscience and strong-field physics, various techniques have been developed to make possible the generation of such high-energy, few-femtosecond pulses [4, 5]. However, not only the generation remains a delicate process, but the complete spectrot temporal pulse characterization calls for methods beyond conventional autocorrelation. Pioneered by Kane and Trebino more than 20 years ago [6], frequency-resolved optical gating (FROG) has established itself as one of the most widely used techniques for ultrashort laser pulse characterization, both in amplitude and phase [5, 7]. Apart from characterization, the control of ultrashort pulses is of key importance in order to exploit their entire potential of application. With the pulse duration approaching a single optical cycle, the light-matter interaction is more and more determined by the behaviour of the carrier wave under the pulse envelope [8]. In particular, the carrier-envelope phase (CEP) – the phase of the carrier wave relative to the envelope maximum – becomes an important parameter, which has to be precisely determined and controlled in order to achieve long-term stability [4, 5] – yet another challenge in ultrashort pulse laser technology.

One widely used technique for the generation of sub-10fs pulses with energies in the millijoule range [9] is hollow-core fiber compression (HFC), which was first demonstrated by Nisoli *et al.* in 1996 [10]. Pulses with durations of the order of 20–30 fs are first coupled into a hollow waveguide filled with noble gas. As per the optical Kerr effect, they induce intensity- and thus time-dependent variations to the refractive index of the gas medium leading to spectral broadening via self-phase modulation (SPM). Copropagation of mutually interacting pulses of different colors can even generate additional bandwidth via cross-phase modulation (XPM) while facilitating the overall control of the spectral shape [11]. However, the different frequency components of the spectrally broadened pulses are spread in time due to dispersion. In order to effectively shorten the pulses, this effect has to be compensated for in a final compression step.

Beyond providing insight into ultrashort pulse laser technology in general and HFC in particular, the objective of the project was twofold:

- Performing a spatiotemporal characterization of the ultrashort pulses generated via HFC, using FROG.
- Constructing an f - $2f$ interferometer and measuring the CEP fluctuations of the Ti:sapphire laser system in use.

The structure of the report is as follows: Sec. 2 outlines the physical principles and techniques most relevant to this project, whereupon Sec. 3 describes the experimental setup. In Sec. 4, the results are presented and discussed. Sec. 5 concludes the report by providing a summary of the project in conjunction with a brief outlook.

2 Physical Principles and Techniques

2.1 Self- and Cross-Phase Modulation in Hollow-Core Fiber Compression

One important consequence of the (non-vanishing) third order nonlinear susceptibility $\chi^{(3)}$ is the optical Kerr effect, i.e. an intensity-dependent refractive index of the form

$$n(I) = n_0 + n_2 I, \quad (1)$$

where n_0 and $n_2 \propto \chi^{(3)}$ denote the linear and nonlinear refractive indices of the medium respectively. In the plane wave approximation, the phase of a laser pulse propagating along the z -direction reads $\phi(z, t) = kz - \omega_0 t = \omega_0 n(t)z/c - \omega_0 t$, where ω_0 is the centre frequency. Note that the refractive index $n(t)$ inherits the time dependence of the pulse intensity $I(t)$ as per Eq. (1), giving rise to self-phase modulation (SPM). The time derivative of $\phi(z, t)$ yields the instantaneous carrier frequency

$$\omega(z, t) = -\frac{\partial \phi}{\partial t} = \omega_0 - \frac{\omega_0}{c} \frac{\partial n}{\partial t} z.$$

Hence, upon propagation through a homogeneous medium of length L , the instantaneous carrier frequency of the pulse shifts by

$$\delta\omega(t) = \omega(t) - \omega_0 = -\frac{\omega_0 n_2}{c} \frac{\partial I}{\partial t} L, \quad (2)$$

generating additional spectral bandwidth $\Delta\omega_{\text{SPM}} = \delta\omega_{\text{max}} - \delta\omega_{\text{min}}$. Note that for $n_2 > 0$, as it is given in most media, the leading edge of the pulse shifts towards red frequencies ($\delta\omega < 0$) while the trailing edge is blue-shifted ($\delta\omega > 0$). However, the thus emerging chirp does not influence the temporal pulse shape.

For a more accurate description of spectral broadening in single-mode gas-filled hollow-core fibers (HFs), the above toy model of SPM has to be somewhat extended; in particular, dispersion effects as well as absorption losses have to be taken into account [12]. Expanding the propagation constant $\beta(\omega)$ around ω_0 ,

$$\beta(\omega) = \beta_0 + \beta_1(\omega - \omega_0) + \beta_2/2(\omega - \omega_0)^2 + \mathcal{O}(\omega - \omega_0)^3 \text{ such that } \beta_n = \partial^n \beta / \partial \omega^n \big|_{\omega_0},$$

the electric field of the pulse can be written as $E \propto A(z, t)F(x, y) \exp[i(\beta_0 z - \omega_0 t)]$, where $A(z, t)$ and $F(x, y)$ denote the slowly varying pulse envelope and the field distribution of the dominant EH₁₁ fiber mode [10] respectively. On the basis of Maxwell's equations the following propagation equation can then be derived as outlined in Ref. [12]:

$$\frac{\partial A}{\partial z} + \beta_1 \frac{\partial A}{\partial t} + \frac{\alpha}{2} A + \frac{i}{2} \beta_2 \frac{\partial^2 A}{\partial t^2} = i\gamma |A|^2 A, \text{ where } \gamma = \frac{\omega_0 n_2}{c A_{\text{eff}}}. \quad (3)$$

Here, $\beta_1 = 1/v_g$ is the reciprocal group velocity of the pulse envelope while group velocity dispersion (GVD) comes into play through β_2 and losses are accounted for by the field attenuation constant α . Note that the nonlinearity parameter γ depends on the effective mode area A_{eff} , which can be calculated from $F(x, y)$. With the interplay between dispersion and SPM being rather complex, Eq. (3) is usually tackled numerically. However, neglecting GVD and assuming Gaussian pulses of peak power P_0 and FWHM Δt , the bandwidth generated via SPM evaluates to [10]

$$\Delta\omega_{\text{SPM}} = 2.86\gamma \frac{P_0}{\Delta t} \frac{[1 - \exp(-\alpha L)]}{\alpha}. \quad (4)$$

As the pulse propagates through a normal dispersive medium characterized by $\beta_2 > 0$, SPM and GVD will lead to spectral and temporal broadening¹ respectively, the latter resulting in an almost rectangular envelope with steep edges [12], where $\partial I/\partial t$ is considerable. Since further $\delta\omega \propto \partial I/\partial t$ as indicated by Eq. (2), new frequency components via SPM are mainly generated near the edges and the pulse develops a nearly linear chirp along its width [12]. Although this linearity can be perturbed by an initial chirp before the HF and losses inside, it facilitates dispersion compensation via a dispersive delay line [9]. The latter delays the red frequency components with respect to the blue ones, thus compressing the pulse duration towards the fundamental Fourier transform limit $\Delta t = 2\pi k/\Delta\omega$, where Δt and $\Delta\omega$ denote the full width at half maximum (FWHM) in time and frequency domain respectively and k depends on the actual pulse shape.

Going back to Eq. (1), it is important to note that $n \equiv n(x, y)$ since $I \propto |F(x, y)|^2$. The thus induced transverse refractive index profile can lead to self-focussing of the laser beam which, in the context of HFC, finally results in the ionization of the gas medium and a strong spatial perturbation of the beam profile. With the critical power P_{cr} for self-focussing scaling as $P_{\text{cr}} \propto 1/n_2$, the nonlinear refractive index has to be controlled such that $P < P_{\text{cr}}$ everywhere inside the HF [13]. As the laser pulse propagates along the HF its power P inevitably decreases, hence allowing for n_2 to be gradually increased in order to retain SPM. Since, in turn, n_2 monotonically increases with gas pressure, the desired gradient of the nonlinear refractive index is readily achieved by maintaining a pressure gradient along the HF [11, 13].

Beyond SPM, two copropagating pulses with different centre frequencies $\omega_{1,2}$ can also modulate their phases one another, an effect which is referred to as cross- (XPM) or induced phase modulation (IPM). A treatment within the slowly varying envelope approximation gives rise to the coupled nonlinear wave equations [14, 15]

$$\frac{\partial A_1}{\partial z} + \beta_{11} \frac{\partial A_1}{\partial t} + \frac{\alpha_1}{2} A_1 + \frac{i}{2} \beta_{21} \frac{\partial^2 A_1}{\partial t^2} = i\gamma_1 [|A_1|^2 + 2|A_2|^2] A_1, \quad (5a)$$

$$\frac{\partial A_2}{\partial z} + \beta_{12} \frac{\partial A_2}{\partial t} + \frac{\alpha_2}{2} A_2 + \frac{i}{2} \beta_{22} \frac{\partial^2 A_2}{\partial t^2} = i\gamma_2 [|A_2|^2 + 2|A_1|^2] A_2, \quad (5b)$$

where $\gamma_i = \omega_i n_2 / c A_{\text{eff}}$, all symbols retain their usual meanings and the additional (second) index represents the pulse travelling at $\omega_{1,2}$. Note the structure on the RHS with the first and second term representing SPM and XPM respectively. Once again, Eqs. (5) call for a numerical solution. In the absence of GVD and losses, the total spectral broadening of pulse i may be estimated² as $\Delta\omega_{i\text{SPM+XPM}} \approx 2.86\gamma_i L(P_i + 2P_k)/\Delta t$, corresponding to a relative bandwidth enlargement of $2P_k/P_i$ when compared with pure SPM [15] as given per Eq. (4) for $\alpha \rightarrow 0$. This estimate is rather generous as it does not take into account group velocity mismatch (GVM), i.e. the fact that $\beta_{11} - \beta_{12} \neq 0$. GVM causes the pulses to eventually walk-off, thus limiting the occurrence of XPM. However, by tuning the initial time delay between the pulses and their peak powers, XPM can considerably enhance the spectral broadening while providing more precise controllability over the spectral shape than SPM alone [11, 14, 15].

¹ In the case of anomalous dispersion, however, SPM and GVD can compensate each other. This can lead to the formation of a so-called soliton, i.e. a pulse that maintains its spectral and temporal width [12].

² Assuming Gaussian pulses (identical FWHM Δt , individual peak powers P_i and P_k , negligible GVM).

2.2 Frequency-Resolved Optical Gating

Frequency-resolved optical gating (FROG) has proven a valuable technique for the complete spectrotemporal characterization of ultrashort laser pulses, revealing both amplitude and phase without significant ambiguities [7]. The pulse to be measured is crossed with a gate pulse in a medium that provides an instantaneous nonlinear response, thus generating the signal field

$$E_{\text{sig}}(t, \tau) = E(t)g(t - \tau), \quad (6)$$

where τ denotes the time delay between the two pulses, $E(t)$ represents the complex envelope of the unknown pulse and $g(t - \tau)$ relates to the gate pulse and the actual nonlinearity in use. E_{sig} is then spectrally resolved as a function of τ , yielding the so-called spectrogram or FROG trace [7]

$$I_{\text{FROG}}(\omega, \tau) \equiv \left| \int_{-\infty}^{\infty} E_{\text{sig}}(t, \tau) e^{-i\omega t} dt \right|^2 \equiv \left| \hat{E}_{\text{sig}}(\omega, \tau) \right|^2. \quad (7)$$

At this point, it may be instructive to draw a parallel between FROG traces and musical scores, both describing frequency and intensity versus time [5, 7]. Eq. (7) can further be rewritten in terms of the Fourier transform $\hat{E}_{\text{sig}}(t, \Omega)$ of the signal field $E_{\text{sig}}(t, \tau)$ in τ ,

$$I_{\text{FROG}}(\omega, \tau) = \left| \int_{-\infty}^{\infty} \int_{-\infty}^{\infty} \hat{E}_{\text{sig}}(t, \Omega) e^{-i\omega t - i\Omega \tau} dt d\Omega \right|^2. \quad (8)$$

Since $E(t) \propto \hat{E}_{\text{sig}}(t, 0)$, we see that, in principle, I_{FROG} determines the pulse under investigation. The hence necessary inversion of Eq. (8) is referred to as the 2-D phase retrieval problem, which, however, is known to essentially always yield unique results [6]. It is usually tackled by the powerful algorithm shown in Fig. 1 (a), which is based on Fourier transforms (FTs) and general projections (GPs) [16]. Starting from an initial guess for $E(t)$, the thus generated signal field $E_{\text{sig}}(t, \tau)$ is Fourier-transformed into the (ω, τ) domain. A GP then replaces the magnitude of $\hat{E}_{\text{sig}}(\omega, \tau)$ by the magnitude of the experimental FROG trace, hence projecting the former onto the set of signal fields $\hat{E}'_{\text{sig}}(\omega, \tau)$ that satisfy Eq. (7). After an inverse FT into the time domain, $\hat{E}'_{\text{sig}}(t, \tau)$ has to be projected onto the set of signal fields satisfying Eq. (6). The related GP involves minimizing the distance metric $\sum_{t, \tau} |\hat{E}'_{\text{sig}}(t, \tau) - E(t)g(t - \tau)|$ with respect to $E(t)$ and the latter then acts as an initial guess for the next iteration.

There exists a whole zoo of FROG schemes which make use of different nonlinearities and experimental geometries. Although FROG appears rather straightforward, specific focus has to be placed on the choice of optical components, ensuring full bandwidth coverage without introducing considerable dispersion [5, 7]. In this project, we employ SHG-FROG in its standard non-collinear geometry [17] as shown in Fig. 1 (b). The pulse under investigation is first split into two replicas by means of a beam splitter (BS). A software-controlled delay stage then introduces the time delay τ between the two pulses. The latter are subsequently focussed onto a beta barium borate crystal (BBO) where non-collinear second harmonic generation (SHG) takes place on the basis of the $\chi^{(2)}$ nonlinearity. Finally, the generated SH signal $E_{\text{sig}} = E(t)E(t - \tau)$ is passed into a spectrometer while the residual fundamental beams are dumped. Note that SHG-FROG inherently produces an ambiguity in time, i.e. $I_{\text{FROG}}(\omega, \tau) = I_{\text{FROG}}(\omega, -\tau)$. In some circumstances, this can lead to convergence problems of the retrieval algorithm [17].

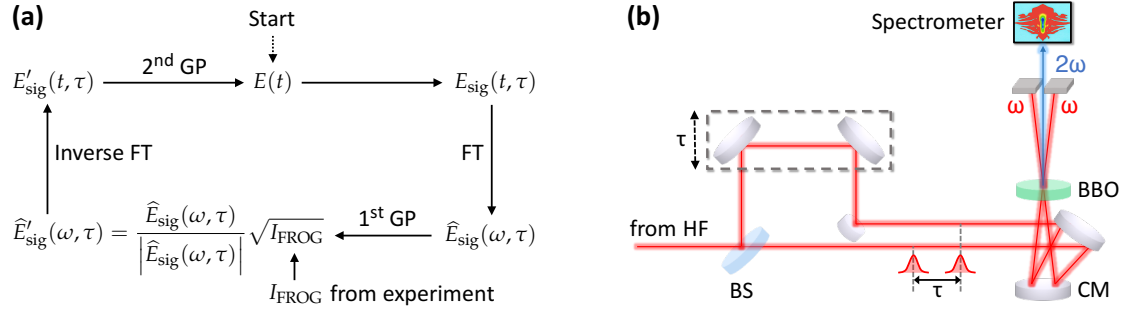


Fig. 1 – Schemes of **(a)** the iterative FROG pulse-retrieval algorithm and **(b)** the standard type of SHG-FROG setup in use within the present project. Adapted from Ref. [7]. **Key:** BS beam splitter, CM concave mirror, BBO beta barium borate crystal.

2.3 Carrier-Envelope Phase and f - $2f$ Interferometry

In the time domain, a mode-locked laser can be schematized as a pulse propagating back and forth inside the cavity and being partially transmitted when it impinges on the output coupler [5]. Since the group (v_g) and phase (v_p) velocities differ inside the cavity, in every roundtrip and thus from pulse to pulse, the carrier-envelope phase (CEP) – the relative phase of the carrier wave with respect to the envelope – shifts by [5]

$$\Delta\phi = 2L \left(\frac{1}{v_g} - \frac{1}{v_p} \right) \omega_0 \bmod 2\pi,$$

where ω_0 denotes the carrier frequency and only the dispersive gain medium of length L has been taken into account. The resulting pulse train is indicated in Fig. 2 (a) and can be written as $E(t) = \sum_m A(t - mT_r) \exp\{i[\omega_0(t - mT_r) + \phi_0 + m\Delta\phi]\} + \text{c.c.}$ [5], where $A(t)$ and ϕ_0 denote the pulse envelope and the initial phase respectively and T_r is the cavity roundtrip time. Transforming this expression into the frequency domain and applying some algebra, one infers that $\hat{E}(\omega) = \hat{A}(\omega - \omega_0) \exp(i\phi_0) \sum_n \delta(\omega - 2\pi n/T_r - \Delta\phi/T_r)$, i.e. the spectrum of the pulse train is a comb of discrete modes at frequencies [5]

$$\omega_n = \frac{2\pi n}{T_r} + \frac{\Delta\phi}{T_r} \text{ or equivalently } \nu_n = n\nu_r + \nu_{\text{CEO}},$$

where $\nu_r = 1/T_r$ is the pulse repetition rate and $\nu_{\text{CEO}} = (\Delta\phi/2\pi)\nu_r$ is the carrier-envelope offset (CEO) frequency. The latter is a direct consequence of the CEP shift $\Delta\phi$, manifesting itself as an offset of the entire frequency comb from integer multiples of ν_r as indicated in Fig. 2 (b). In general, both $\Delta\phi$ and ν_{CEO} are subject to fluctuations and drifts of the laser oscillator parameters, thus causing the CEP to arbitrarily vary in time.

With the pulse duration approaching the time scale of one carrier wave oscillation, it is the electric field rather than the pulse envelope which governs the light-matter interaction, turning the CEP into an important parameter [8]. Although the absolute CEP remains experimentally inaccessible, it is well possible to measure its fluctuations, i.e. ν_{CEO} , by means of f - $2f$ interferometry [5]. This self-referencing technique calls for an optical spectrum spanning at least one octave, the frequency comb thus containing both frequencies $\nu_n = n\nu_r + \nu_{\text{CEO}}$ and $\nu_{2n} = 2n\nu_r + \nu_{\text{CEO}}$. Frequency-doubling the lower frequencies $\nu_n \rightarrow 2\nu_n = 2n\nu_r + 2\nu_{\text{CEO}}$ and overlapping them with the higher frequency part of the fundamental comb, a beat note at $\nu_{\text{CEO}} = 2\nu_n - \nu_{2n}$ can finally be observed.

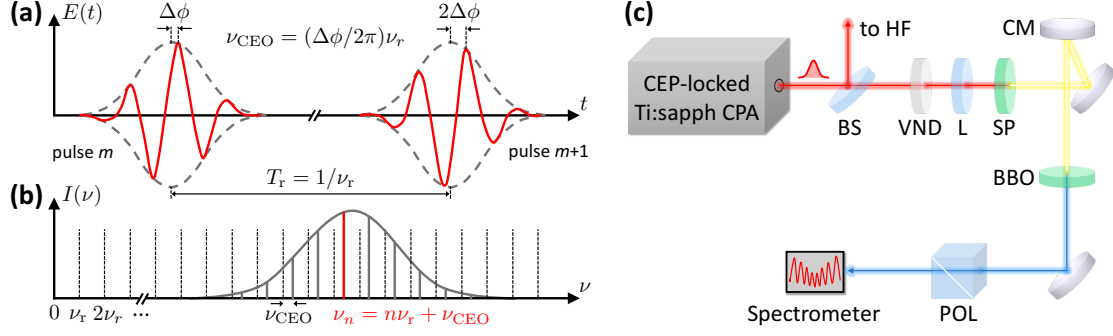


Fig. 2 – (a, b) Time-frequency correspondence between the pulse-to-pulse CEP shift $\Delta\phi$ and the CEO frequency ν_{CEO} . Adapted from Ref. [18]. **(c)** Schematic of the constructed f - $2f$ interferometer allowing for the characterization of CEP fluctuations on a single-shot basis. **Key:** BS beam splitter, VND variable neutral density filter, L focussing lens, SP sapphire plate, CM concave mirror, BBO beta barium borate crystal, POL polarizer.

Fig. 2 (c) shows the schematic setup of the f - $2f$ interferometer that has been constructed within the framework of the present project. Based on the configuration initially proposed by Kakehata *et al.* in 2001 [19], it allows – in principle – for a direct measurement of the CEP fluctuations of the employed Ti:sapphire laser system (see Sec. 3) on a shot-to-shot basis. In order to protect the nonlinear optical components, only a negligible amount of the total pulse energy is coupled into the interferometer where a variable neutral density filter (VND) allows for further attenuation. The pulses are then focussed onto a 1 mm-thick sapphire plate (SP) generating a white-light continuum (WLC) which extends over more than one octave. Subsequently, the low-frequency part of the WLC is frequency-doubled in a 0.5 mm-thick type-I BBO, such that the SH spectrally overlaps with the high-frequency part of the collinearly propagating fundamental (FF). The FF and SH are then projected onto a common axis of polarization by means of a polarizer (POL). Finally, they enter a spectrometer where an interference pattern is observed in the region of spectral overlap. The related spectral intensity reads [5]

$$I(\omega) = |\hat{E}_{\text{FF}}(\omega)|^2 + |\hat{E}_{\text{SH}}(\omega)|^2 + 2|\hat{E}_{\text{FF}}(\omega)||\hat{E}_{\text{SH}}(\omega)|\cos(\omega\tau + \Delta\phi), \quad (9)$$

where τ denotes the delay between the FF and SH pulses. Since the CEP shift $\Delta\phi$ varies from pulse to pulse, the interference fringes will move accordingly, thus providing access to the CEP fluctuations through the FT of the fringe pattern (9) [5, 19].

Being important for applications such as high harmonic generation [4] or coherent waveform synthesis [5], pulse trains with stable CEP are usually created using an active approach [5, 18]. Here, ν_{CEO} is first measured after the laser oscillator by means of the conventional self-referencing technique as described further above. The CEO frequency is then locked to $\nu_{\text{CEO}}^* = \nu_r/n$ – an integer fraction of the oscillator frequency ν_r – via an active feedback loop; every n -th pulse is thus guaranteed to have the same CEP. Picking pulses at again an integer fraction of ν_{CEO}^* (as it naturally occurs if the pulses get amplified) then yields a CEP-stabilized pulse train with a repetition rate at the order of 1 kHz. In order to correct for CEP fluctuations induced in the (optional) amplification process, an additional feedback loop based on single-shot f - $2f$ interferometry can be used to act on the amplifier. This procedure enables the generation of high-energy pulse trains with root mean square CEP fluctuations of the order of 100 to 200 mrad [5, 20].

3 Experimental Setup

At the heart of the setup (see Fig. 3) is a CEP-locked Ti:sapphire chirped-pulse amplification³ (CPA) laser system consisting of the following main components:

- A frequency-doubled Nd:YLF pulsed pump laser (Coherent® Revolution family) with an average output power of 65 W, pumping
- an ultrashort pulse Ti:sapphire oscillator (Coherent® Vitara family) equipped with an active feedback loop CEP stabilizer. The oscillator in turn seeds
- a regenerative chirped-pulse amplifier (Coherent® Legend Elite series). Here, the CEP-stable pulses from the oscillator are first stretched out temporally using a pair of gratings. The thus reduced peak power enables pulse amplification in a Ti:sapphire crystal. Finally, the pulses are recompressed by another grating pair.

The laser system delivers p-polarized, 5 mJ, 30 fs pulses at a centre wavelength of 800 nm with a repetition rate of 3 kHz. The intensity is first equally distributed onto two channels by a 50:50 BS. One channel essentially serves for free-space pulse propagation with only a tiny amount of intensity being outcoupled into the single-shot f -2 f interferometer described in Sec. 2.3, Fig. 2(c). The other channel is dedicated to SHG in a 0.5 mm-thick type-I BBO; an additional half-wave plate (HWP) ensures that the generated SH is also p-polarized. Two harmonic separators (HS) mounted onto a delay stage are then used to filter out the residual FF pulses. In order to facilitate the later coupling of the FF and SH pulses into the HF, each channel further contains

- a biconvex lens (L) of focal length 1.5 m for the FF and 2 m for the SH respectively, focussing the beam onto the HF entrance.
- two piezoelectric-actuated mirrors (ACs) to stabilize the alignment of the beam with the HF. The ACs are dynamically adjusted based on the feedback signal of a photodiode, which measures the fluctuations in the laser beam pointing.⁴

Eventually, both channels are recombined by a beam combiner (BC) and the pulses enter the HF (length $L = 1$ m, radius $a = 300 \mu\text{m}$) with an adjustable time delay Δt between the FF (pulse energy ≈ 2 mJ) and the SH ($\approx 400 \mu\text{J}$). The HF is filled with neon at a constant pressure of 2 bar (unless explicitly stated otherwise) and surrounded by a glass tube sealed with 1 mm-thick calcium fluoride Brewster windows. As discussed in Sec. 2.1, SPM and IPM lead to spectral broadening inside the HF. At the current stage, however, only the FF pulses are coupled into the fiber whereas the SH channel is blocked (unless explicitly stated otherwise). Inevitable losses reduce the output pulse energy to around 1 mJ, irrespective of whether the SH is present. After the HF, the pulses perform 5 bounces between two double-chirped mirrors³ (DCMs). These allow for dispersion compensation in the wavelength regime between 650 and 950 nm by delaying the red frequencies with respect to the blue ones, thus compressing the pulses towards the Fourier transform limit as determined by the enhanced spectral bandwidth. Finally, the pulses can either be characterized via SHG FROG as outlined in Sec. 2.2 or serve as the basis for another experiment. One such application is high harmonic generation, which is however beyond the scope of the present project.

³ See Refs. [21, 22] for more details on chirped-pulse amplification and double-chirped mirrors.

⁴ For this purpose, a tiny amount of intensity is coupled out of each path; this is not indicated in Fig. 3.

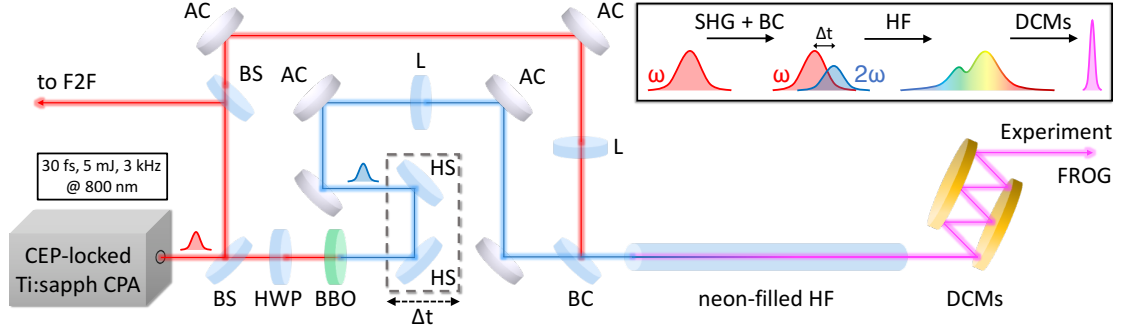


Fig. 3 – Schematic setup for the generation of ultrashort pulses using a CEP-locked Ti:sapphire CPA laser system and hollow-core fiber compression based on SPM and IPM. See text for description. **Inset:** Schematic evolution of the laser pulses as they propagate through the setup. **Key:** *BS* beam splitter, *HWP* half-wave plate, *BBO* beta barium borate crystal, *HS* harmonic separator, *AC* piezoelectric-actuated mirror, *L* focusing lens, *BC* beam combiner, *HF* hollow-core fiber, *DCMs* double chirped mirrors.

4 Results and Discussion

4.1 Spectral Broadening inside the Hollow-Core Fiber

The FF pulse spectrum undergoes considerable broadening upon propagation through the HF as can be seen when comparing the red and blue curve in Fig. 4. Here, only the FF pulses were coupled into the HF. The output spectrum ranges from around 600 nm to 970 nm, corresponding to a bandwidth of $\Delta\omega = 1.2 \times 10^{15}$ rad/s, which almost exceeds the initial bandwidth by one order of magnitude. In order to compare this experimental result with the simplified version of the SPM theory as outlined in Sec. 2.1, the following parameters are employed:

- the field attenuation constant $\alpha = 0.7 \text{ m}^{-1}$, which is given by $\exp(-\alpha L) = 0.5$,⁵
- the effective mode area $A_{\text{eff}} = 0.477\pi a^2 = 0.034 \text{ mm}^2$ [11],
- the nonlinear refractive index of neon at 2 bar: $n_2 = 1.75 \times 10^{-20} \text{ cm}^2/\text{W}$ [23],
- the pulse peak power $P_0 \approx \text{pulse energy}/\text{duration} = 6.7 \times 10^{10} \text{ W}$.

Substituting the above into Eq. (4), the total bandwidth $\Delta\omega_{\text{SPM}}$ generated from SPM can be estimated as 1.8×10^{15} rad/s. The considerable difference between $\Delta\omega_{\text{SPM}}$ and the experimental result can be understood from the fact that Eq. (4) is a tremendous simplification of the modelling of spectral broadening in HFs; in particular, the neglect of dispersion-induced pulse broadening contributes to the overestimate of $\Delta\omega$. However, the bandwidth is predicted to the correct order of magnitude, indicating that SPM indeed is the dominant nonlinear process inside the HF. If additionally the SH is coupled into the fiber, XPM leads to an enhancement of the spectral broadening as can be seen from the green curve in Fig. 4. The combined spectrum of both pulses ranges from around 320 nm to 970 nm with the individual spectra overlapping in a

⁵ $\exp(-\alpha L) = 0.5$ since the pulse energy decreases from 2 mJ to 1 mJ inside the HF.

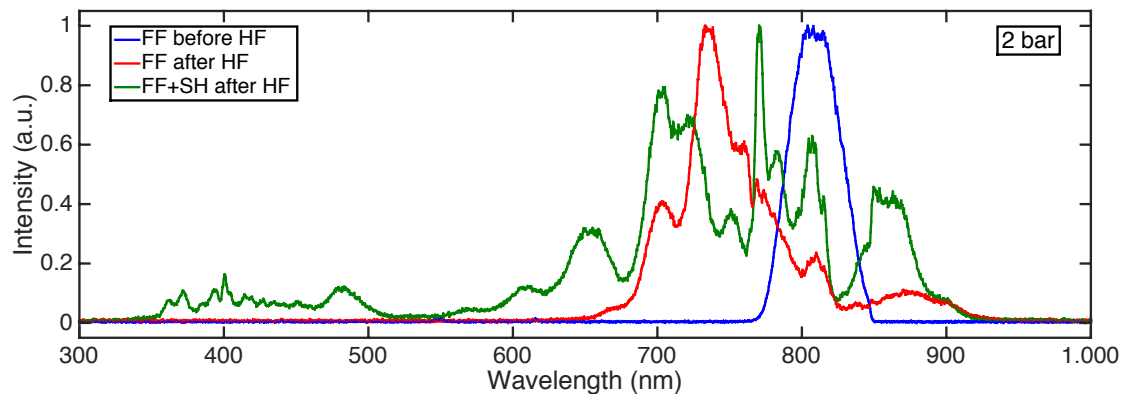


Fig. 4 – Upon propagation through the HF, the FF pulse spectrum (blue curve) is broadened (red curve), most notably through SPM. If, in addition, the frequency-doubled pulses are coupled into the HF, the spectral broadening is further enhanced as a consequence of XPM between the FF and the SH.

40 nm-broad region centered around 530 nm. Compared to the case of sole SPM, the bandwidth of the FF increases by about 30 % to 1.6×10^{15} rad/s. Assuming identical durations of the FF and SH pulse, the simple theory of XPM – neglecting dispersion and group velocity mismatch (see Sec. 2.1) – predicts a relative bandwidth increase of 40 %, which agrees surprisingly well with the observed value. However, the complex interplay of dispersion, SPM (and IPM) and other potential nonlinear effects turns spectral broadening of high-energy, ultrashort pulses in HFs into a nontrivial phenomenon. While the simple theory outlined in Sec. 2.1 can provide an intuitive picture of the underlying physics, many of its foundations – such as the slowly varying envelope approximation – start to break down with shorter and shorter pulse durations and other nonlinear effects become considerable at higher and higher intensities [24].

Fig. 5(a) shows 10 spectra measured at different gas pressures between 0 and 2 bar inside the HF. Extracting the respective spectral bandwidth, it turns out that an exponential dependence of $\Delta\omega$ on the gas pressure provides the best fit to the experimental data as it is shown in Fig. 5(b). Since the nonlinear refractive index n_2 is proportional to the gas pressure [13, 23], one would rather expect a linear increase of $\Delta\omega$ with gas pressure. This linear behaviour has indeed been observed in previous studies by Wang *et al.* [23]; however, the present experiment uses pulses of both higher energy and shorter duration, such that a direct comparison with the above work is rather pointless. Amongst other effects, ionization of the gas atoms is known to influence the linear pressure dependence of the bandwidth [25]. In the present experiment, however, the pulse peak power at the HF entrance exceeds the critical power $P_c = \lambda^2/2\pi n_2$ [10] for self-focussing. Against this background, ionization effects have to be taken into account. Note further that the broadened spectra are no longer symmetric around their center wavelength and blue-shifted with respect to the initial FF spectrum. This is a well-known consequence of self-steepening, i.e. a change in the pulse shape induced by the intensity-dependent refractive index. In order to examine the actual influence of ionization and self-steepening on the spectral bandwidth, one would have to extend the propagation equation – the interested reader shall be referred to Ref. [24] – and perform numerical simulations; this lies beyond the scope of the present project.

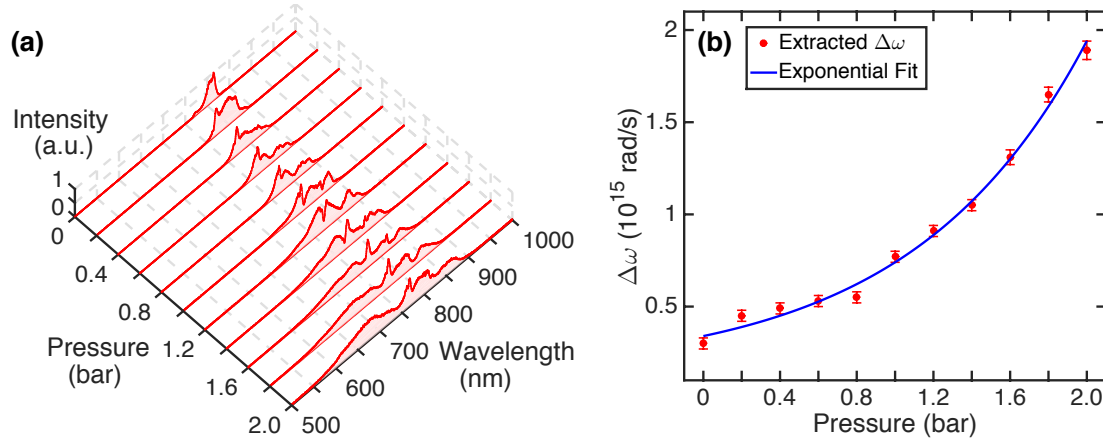


Fig. 5 – The FF spectrum is observed to become more and more broadband with increasing gas pressure inside the HF (a). Based on the simple theory of SPM, one would expect the generated bandwidth $\Delta\omega$ to be proportional to the gas pressure. However, $\Delta\omega$ seems to rather follow an exponential dependence, indicating that the pulse propagation inside the HF is influenced by other (nonlinear optical) effects (b).

4.2 Spectrotemporal Pulse Characterization

While multiple FROG traces have been measured using the noncollinear SHG geometry (see Sec. 2.2, Fig. 1 (b)), only one complete reconstruction will be presented here for the sake of brevity. The corresponding measurement was performed at a gas pressure of 2.2 bar inside the HF and the pulses were passed through a 1 mm-thick fused silica plate⁶ after having been compressed via the pair of DCMs.

Comparing Figs. 6(a) and (b), one notes the overall good agreement between the measured and the retrieved FROG trace; the computed error corresponds to 0.5 %. The reconstructed temporal pulse shape is shown in Fig. 6(c). With a FWHM of 7.1 fs this is, to the best of the author's knowledge, the shortest pulse produced by the present setup. Note that the phase appears almost flat along the main intensity peak and thus, the pulse is already close to the fundamental Fourier transform limit (TL) corresponding to a FWHM of 5.9 fs. The TL pulse has been computed by Fourier transforming the measured pulse spectrum shown in Fig. 6(d). Comparing the latter with the reconstructed spectrum, one notes the good agreement between the spectral shapes. The deviations in relative intensity are mainly due to the non-uniform response of the spectrometer over the entire range of wavelengths and can thus be eliminated by applying a marginal correction to the retrieved spectrum. The employed DCMs are able to compensate for dispersion in the wavelength regime between 650 and 950 nm, such that the spectral phase is indeed reconstructed as almost flat along the entire pulse spectrum. However, phase jumps around 700 and 850 nm can still be identified as the main contribution to the difference between the reconstructed and the TL pulse duration. In addition to the observed nonlinear pressure dependence of the spectral bandwidth (see Sec. 4.1), these jumps suggest the presence of further, not yet clearly identified processes beyond SPM and dispersion inside the HF.

⁶ This simulates the entrance window to the vacuum chamber inside of which the pulses will eventually be used to trigger high harmonic generation.

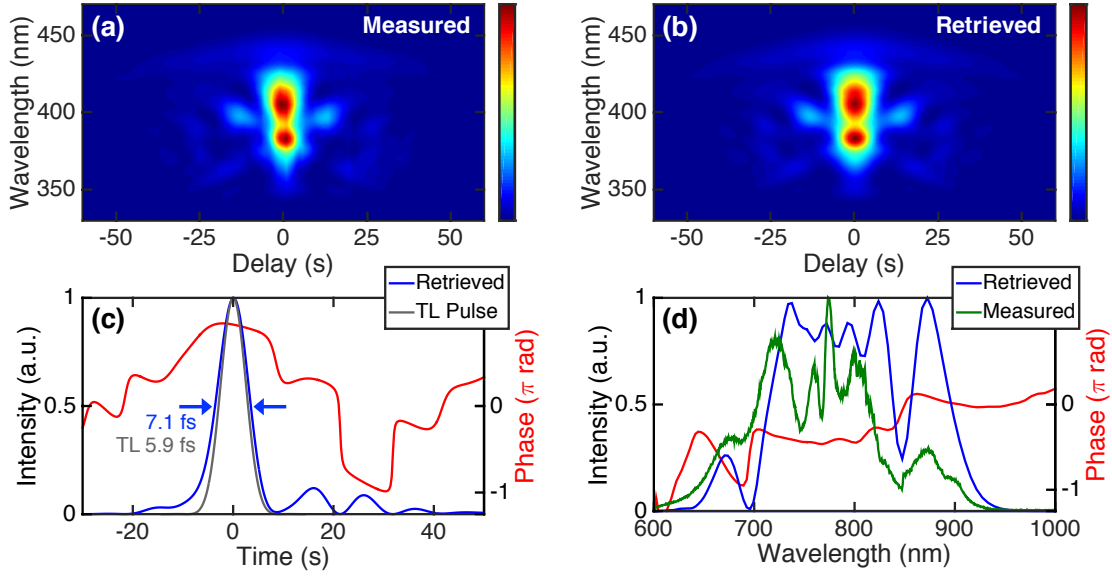


Fig. 6 – Example of a spectrotemporal FROG characterization. The error between the measured (a) and the retrieved FROG trace (b) amounts to 0.5 %. The retrieved pulse duration of 7.1 fs is already close to the TL of 5.9 fs (c). The retrieved and measured spectrum demonstrate good agreement, while phase jumps around 700 and 850 nm point towards processes other than SPM and pure dispersion inside the HF (d).

4.3 Carrier-Envelope Phase Fluctuations

The CEP fluctuations of the CEP-locked Ti:sapphire CPA system have been measured by guiding a negligible amount of intensity into the collinear f - $2f$ interferometer, which has been set up as described in Sec. 2.3. The BBO crystal was phasematched such that the short-wavelength part of the WLC overlapped with the long wavelength-part of the SH. After the precise alignment of all components, spectral fringes became visible in the range between 490 and 550 nm, as can be seen from Figs. 7 and 8 (a). By acquiring a series of spectra, the phase shift $\Delta\phi$ as a function of time can then be extracted from the temporal evolution of the fringe pattern (see Figs. 7 and 8 (b)). The integration time of the spectrometer is however limited to 1 ms, such that each measured spectrum is the actual average of 2 or 3 consecutive pulses. Since the data transfer from the spectrometer takes another 1 ms, 2 to 3 pulses are omitted between consecutive spectra.

Fig. 7 illustrates the CEP fluctuations over a duration of 2 s. In this measurement, the CEP demonstrates good stability with a root mean square⁷ (RMS) of 550 mrad. When compared to relevant literature [5, 20, 26], this value still seems rather high – however, one cannot readily attribute these fluctuations solely to the laser system itself. On the one hand, since the employed spectrometer is designed to cover a broad wavelength range, its resolution is somewhat limited. Therefore, every single fringe is supported by only few data points and the minimal resolvable CEP jitter might well exceed the actual fluctuations. On the other hand, the setup has not been entirely shielded from the environment during data acquisition such that the fringe pattern could have been perturbed by air drafts or mechanical influence. Last but not least, the employed f - $2f$

⁷ For n data points $\Delta\phi_n$ with a mean value of $\overline{\Delta\phi}$, the RMS is given as $[(1/n) \sum_n (\Delta\phi_n - \overline{\Delta\phi})^2]^{1/2}$.

setup itself is known to affect $\Delta\phi$ on the order of 100 mrad based on fluctuations in the laser pulse energy (referred to as phase-energy coupling) [26]. When extending the duration of measurement to 20 s, slow CEP drifts become apparent as shown in Fig. 8 (b, d) and the RMS increases to 930 mrad. This phenomenon is rather trivial since, in the present setup, only the oscillator is CEP-stabilized whereas the amplifier is not acted upon by a slow-feedback loop. Ignoring these slow drifts, the RMS still exceeds the value of the 2 s-long measurement. This indicates that indeed the spectral resolution, which is decreased here due to narrower fringes (see Figs. 7 and 8 (a)), might limit the achievable precision of the CEP measurement.

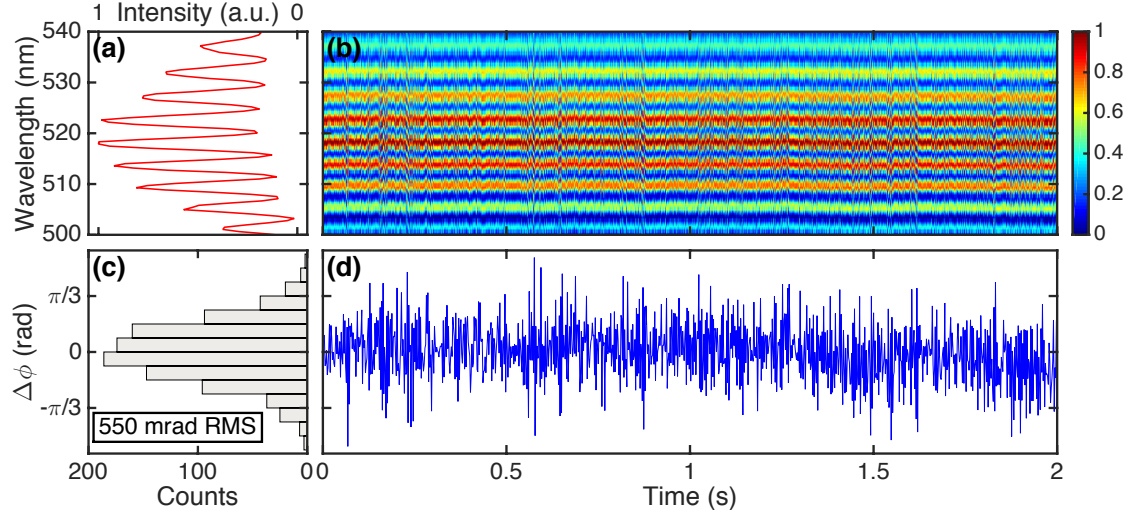


Fig. 7 – Using an f -2 f interferometer, spectral fringes are observed in the region around 520 nm (a). From the temporal evolution of the fringe pattern over 2 s (b), the CEP phase shift $\Delta\phi$ can be extracted and the fluctuations can be monitored over time (c, d). Note that this is not a proper single-shot measurement due to limitations of the spectrometer.

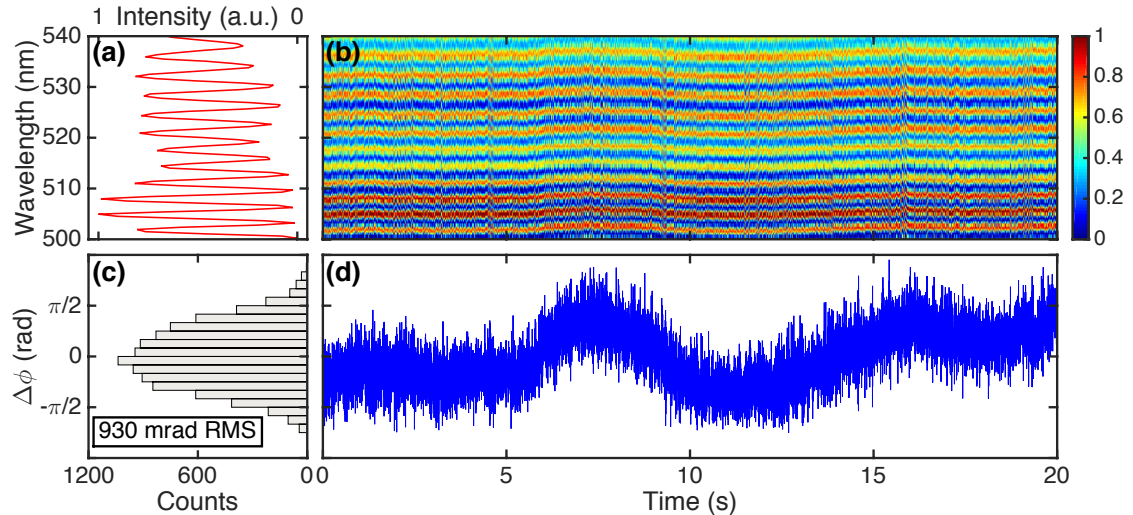


Fig. 8 – On a time scale of 20 s, slow CEP drifts are identified (b, d) due to the absence of a slow-loop feedback acting on the laser amplifier. Note the narrower fringes (a) and the thus decreased spectral resolution in comparison with the 2 s-long measurement.

5 Summary and Outlook

By coupling the 30 fs pulses of a carrier-envelope phase-stabilized Ti:sapphire amplifier system into a neon-filled hollow-core fiber, the initial pulse spectrum has been demonstrated to broaden by almost one order of magnitude to above 10^{15} rad/s; the generated bandwidth can mainly be attributed to self-phase modulation inside the fiber. An exponential increase in bandwidth with gas pressure has been observed, whereas the theory of pure self-phase modulation predicts a linear dependence. This indicates that the pulse propagation inside the fiber is influenced by further processes, which have yet to be clearly identified. In fact, both the asymmetry and blue-shift of the broadened spectrum point towards self-steepening, while ionization effects have to be taken into account due to the pulse peak power exceeding the critical value for self-focussing at the fiber entrance. In further studies one could establish a pressure gradient along the fiber in order to reduce the potential influence of ionization on the generated bandwidth. Likewise, in order to substantiate the experimental results with an appropriate model of pulse propagation, simulations will have to be performed, encompassing potential (nonlinear) effects beyond self-phase modulation and dispersion.

After compression of the spectrally and temporally broadened pulses via a pair of double-chirped mirrors, they have been fully characterized using frequency-resolved optical gating based on second-harmonic generation. A full width at half maximum duration of 7.1 fs has been retrieved, which is in fact the shortest pulse duration generated with the present setup. Both the temporal and spectral phases have been found to be flat over the respective region of interest, being consistent with the fact that the generated pulses are close to the computed Fourier transform limit of 5.9 fs. Small phase jumps can still be identified, serving as yet another argument for additional processes happening inside the hollow-core fiber. One possible route towards even shorter pulses could be cross-phase modulation between differently colored pulses inside the fiber; in fact, the present study has seen the bandwidth of the pulses increase by another 30 % upon copropagation with their frequency-doubled replicas. However, in order to benefit from this enhanced bandwidth in terms of shorter pulses, the present setup has to be equipped with double-chirped mirrors covering a broader wavelength range or with even other compression schemes on the basis of spatial light modulators.

The carrier-envelope phase fluctuations of the employed laser system have been characterized using a self-constructed f - $2f$ interferometer. Since the minimal integration time of the employed spectrometer captures at least 2 pulses, the performed measurements only provide an estimate of the actual shot-to-shot fluctuations. Moreover, due to the broadband character of the spectrometer, the achievable spectral resolution and the thus retrieved phase fluctuations might exceed the jitter introduced by the laser system itself. On a 2 s timescale, the carrier-envelope phase turned out to be stable with a root mean square deviation of 550 mrad. On a 20 s timescale, however, slow drifts have been identified originating from the laser amplifier, which is not acted upon by a slow feedback loop. The latter could well be set up on the basis of the constructed f - $2f$ interferometer. Future studies should improve the temporal and spectral resolution of the f - $2f$ setup, aiming for a precise characterization of carrier-envelope phase fluctuations at the fiber output. These could shed light on the physics beyond conventional self-phase modulation inside the fiber and thus eventually complete the circle.

References

1. Maiman, T. H. Stimulated Optical Radiation in Ruby. *Nature* **187**, 493–494 (1960).
2. Ippen, E. P., Shank, C. V. & Dienes, A. Passive mode locking of the cw dye laser. *Appl. Phys. Lett.* **21**, 348–350 (1972).
3. Kärtner, F. X. *et al.* Few-Cycle Pulses Directly from a Laser. In *Few-Cycle Laser Pulse Generation and Its Applications* (ed. Kärtner, F. X.) (Springer, Berlin, 2004).
4. Krausz, F. & Ivanov, M. Attosecond physics. *Rev. Mod. Phys.* **81**, 163–234 (2009).
5. Manzoni, C. *et al.* Coherent pulse synthesis: towards sub-cycle optical waveforms. *Laser Photon. Rev.* **9**, 129–171 (2015).
6. Kane, D. J. & Trebino, R. Characterization of Arbitrary Femtosecond Pulses Using Frequency-Resolved Optical Gating. *IEEE J. Quantum Electron.* **29**, 571–579 (1993).
7. Trebino, R. *Frequency-Resolved Optical Gating: The Measurement of Ultrashort Laser Pulses* (Springer, New York, 2000).
8. Brabec, T. & Krausz, F. Intense few-cycle laser fields: Frontiers of nonlinear optics. *Rev. Mod. Phys.* **72**, 545–591 (2000).
9. DeSilvestri, S., Nisoli, M., Sansone, G., Stagira, S. & Svelto, O. Few-Cycle Pulses by External Compression. In *Few-Cycle Laser Pulse Generation and Its Applications* (ed. Kärtner, F. X.) (Springer, Berlin, 2004).
10. Nisoli, M., De Silvestri, S. & Svelto, O. Generation of high energy 10 fs pulses by a new pulse compression technique. *Appl. Phys. Lett.* **68**, 2793–2795 (1996).
11. Fang, S. *et al.* Generation of Sub-900- μ J Supercontinuum With a Two-Octave Bandwidth Based on Induced Phase Modulation in Argon-Filled Hollow Fiber. *IEEE Phot. Tech. Lett.* **23**, 688–690 (2011).
12. Agrawal, G. P. Ultrashort Pulse Propagation in Nonlinear Dispersive Fibers. In *The Supercontinuum Laser Source* (ed. Alfano, R. R.) 2nd ed. (Springer, New York, 2006).
13. Nurhuda, M., Suda, A., Midorikawa, K., Hatayama, M. & Nagasaka, K. Propagation dynamics of femtosecond laser pulses in a hollow fiber filled with argon: constant gas pressure versus differential gas pressure. *J. Opt. Soc. Am. B* **20**, 2002–2011 (2003).
14. Karasawa, N., Morita, R., Xu, L., Shigekawa, H. & Yamashita, M. Theory of ultrabroadband optical pulse generation by induced phase modulation in a gas-filled hollow waveguide. *J. Opt. Soc. Am. B* **16**, 662–668 (1999).
15. Baldeck, P. L., Ho, P. P. & Alfano, R. R. Cross-Phase Modulation: A New Technique for Controlling the Spectral, Temporal, and Spatial Properties of Ultrashort Pulses. In *The Supercontinuum Laser Source* (ed. Alfano, R. R.) 2nd ed. (Springer, New York, 2006).
16. DeLong, K. W., Kohler, B., Wilson, K., Fittinghoff, D. N. & Trebino, R. Pulse retrieval in frequency-resolved optical gating based on the method of generalized projections. *Opt. Lett.* **19**, 2152–2154 (1994).
17. DeLong, K. W., Trebino, R., Hunter, J. & White, W. E. Frequency-resolved optical gating with the use of second-harmonic generation. *J. Opt. Soc. Am. B* **11**, 2206–2215 (1994).

18. Jones, D. J. *et al.* Carrier-Envelope Phase Control of Femtosecond Mode-Locked Lasers and Direct Optical Frequency Synthesis. *Science* **288**, 635–639 (2000).
19. Kakehata, M. *et al.* Single-shot measurement of carrier-envelope phase changes by spectral interferometry. *Opt. Lett.* **26**, 1436–1438 (2001).
20. Li, C. *et al.* Precision control of carrier-envelope phase in grating based chirped pulse amplifiers. *Opt. Express* **14**, 11468–11476 (2006).
21. Strickland, D. & Mourou, G. Compression of amplified chirped optical pulses. *Opt. Commun.* **56**, 219–221 (1985).
22. Kärtner, F. X. *et al.* Design and fabrication of double-chirped mirrors. *Opt. Lett.* **22**, 831–833 (1997).
23. Wang, D., Leng, Y. & Xu, Z. Measurement of nonlinear refractive index coefficient of inert gases with hollow-core fiber. *Appl. Phys. B* **111**, 447–452 (2013).
24. Aközbek, N. *et al.* Extending the supercontinuum spectrum down to 200 nm with few-cycle pulses. *New J. Phys.* **8**, 177 (2006).
25. Bohman, S., Suda, A., Kanai, T., Yamaguchi, S. & Midorikawa, K. Generation of 5.0 fs, 5.0 mJ pulses at 1 kHz using hollow-fiber pulse compression. *Opt. Lett.* **35**, 1887–1889 (2010).
26. Li, C. *et al.* Determining the phase-energy coupling coefficient in carrier-envelope phase measurements. *Opt. Lett.* **32**, 796–798 (2007).

Acknowledgements

At this point I would like to express my sincere gratitude to all the people and institutions who have contributed to this project in the framework of the DESY Summer Student Program. I owe special thanks to:

Dr. Shaobo Fang and **Dr. Liwei Song** for not only supervising and guiding me with great expertise but also for infecting me with their enthusiasm for ultrafast optics.

Dr. Giovanni Cirmi for his help with the FROG data evaluation and **Dr. Oliver Mücke** for discussing some of the results and providing reference to relevant literature.

Prof. Dr. Franz Kärtner for hosting me as a DESY Summer Student in his group at the Center for Free-Electron Laser Science. It has been a most valuable experience.

The entire **Ultrafast Optics and X-Rays Division** at CFEL who always made me feel welcome and have created a friendly working atmosphere. In particular, I am grateful to **Mr. Koustuban Ravi**, **Dr. François Lemery** and my fellow interns **Mr. Thomas Braatz**, **Ms. Emma Kueny** and **Ms. Lu Wang** for valuable discussions both at and after work and, not least, numerous culinary adventures.

Prof. Dr. Thomas Fauster and **Dr. Derek Lee** for supporting my application to the DESY Summer Student Program.

My parents and **Ms. Meltem Ivren** for the great support in general and for proofreading this report in particular.

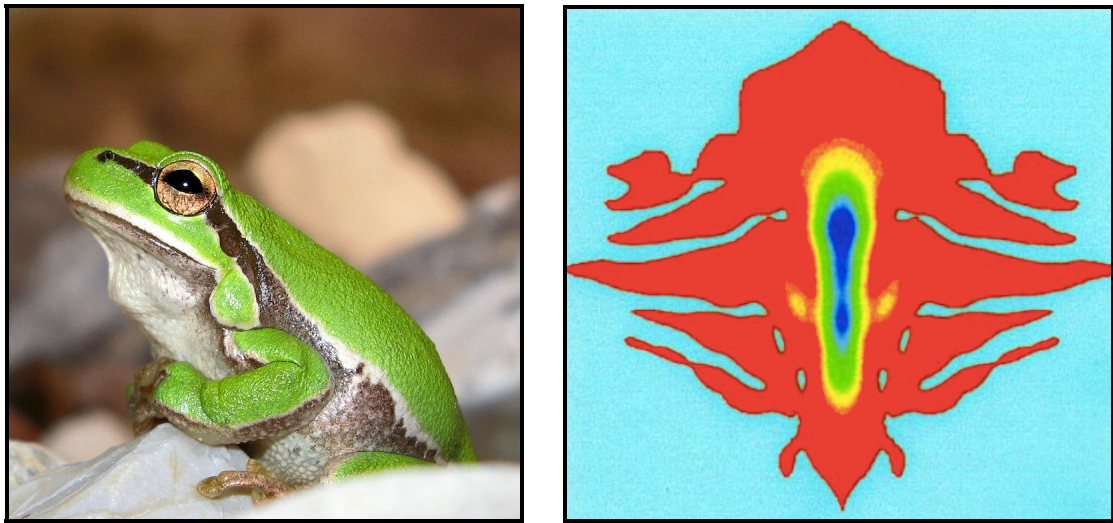


Fig. 9 – The European tree frog (*Hyla arborea*) (**left**) can grow up to 5 cm in length⁸ while FROG (**right**) can characterize laser pulses with durations of only a few fs. FROG trace adapted from Baltuška *et al.*, J. Quant. Electron. **35**, 459–478 (1999).

⁸ See https://en.wikipedia.org/wiki/European_tree_frog. Image: Copyright by Ester Inbar, available from <http://commons.wikimedia.org/wiki/User:ST>.